Variational Assimilation of SSM/I Total Precipitable Water Retrievals in the CMC Analysis System

GODELIEVE DEBLONDE

Data Assimilation and Satellite Meteorology Division, Atmospheric Environment Service, Dorval, Quebec, Canada

(Manuscript received 2 March 1998, in final form 10 July 1998)

ABSTRACT

The impact of assimilating Special Sensor Microwave/Imager (SSM/I) total precipitable water (TPW) on the Canadian Meteorological Centre (CMC) operational analyses and forecasts is evaluated. Assimilation cycles were performed for the months of July 1996 and December 1996. The agreement between the SSM/I TPW climatology and the analyzed TPW for the control case (for which only conventional observations were assimilated) was quite good (root-mean-square difference of 2.8 kg m^{-2}), which showed that the humidity analysis for the control case was already good. As a result of assimilating SSM/I TPW and depending on the month studied, collocations with radiosondes over the oceans showed that both the analyses and the 6-h forecasts of humidity were improved in the Tropics and to a lesser degree in the Southern Hemisphere extratropics. The geopotential anomaly correlations that were computed only for the July 1996 case showed an increase of 1%–2% starting with the day 3 forecast in the Tropics and the day 4 forecast in the Southern Hemisphere extratropics.

Comparison with precipitation climatological observations indicated that the CMC spectral finite element (SEF) global forecast model (which has a considerable precipitation spinup) has a hydrological cycle that is too active. The precipitation that occurs in the intertropical convergence zone (ITCZ) and South Pacific convergence zone covers an area that is too wide and the size of the areas where large-scale subsidence occurs are greatly underestimated. The net impact of assimilating SSM/I TPW was to slightly reduce the globally averaged precipitation rate and thus bring the 6-h forecasts closer to the observations. The precipitation rates were mainly decreased in the Southern Hemisphere (where the SEF model is shown to have a wet bias) and increased where the maximum ITCZ precipitation occurs. The precipitation in the large-scale subsidence zones was also reduced in agreement with the observations. The residence time of the impact of the SSM/I TPW was fairly short: about 24 h in the midlatitudes and 48 h in the Tropics. Although the humidity analysis was univariate, assimilating SSM/I TPW accelerated the Hadley cell and increased the meridional transport of humidity in the Tropics.

1. Introduction

Over the oceans, the number of conventional humidity observations is extremely limited. A source of humidity measurements with high spatial and temporal resolution is available from satellite observations. These observations however measure humidity indirectly. Three techniques currently exist to extract humidity from these observations. First, a retrieval technique can be used to derive humidity from satellite observations in the same form as conventional observations. These retrievals are then assimilated in the same way as conventional observations to produce analyses. Second, radiances are assimilated directly into a variational analysis system. Essentially, humidity profiles are iterated upon until a best agreement in a least squares sense is found between observed and simulated radiances. Short-term forecasts are used as a first guess. The resulting humidity profiles then form the analyses. Third, a hybrid technique is used between the two techniques just described. This hybrid technique is used when the geophysical variable retrieved is not a control variable of the assimilation system. In the case of Special Sensor Microwave/Imager (SSM/I) total precipitable water (TPW), the process may be summarized as follows. In a first step, TPW over the oceans is derived from SSM/I brightness temperatures (TB) using a regression equation (e.g., Alishouse et al. 1990; Petty 1990). The root-mean-square differences (rmsd's) of the retrievals w.r.t. radiosonde measurements is around 4 kg m^{-2} (Deblonde and Wagneur 1997). The retrieved TPW is then assimilated using a simulator operator for TPW that is simply the integral operator since TPW is the vertical integral of specific humidity.

The retrievals obtained from a regression equation are computationally cost efficient. TPW obtained in such a fashion has been assimilated in global analysis systems by Ledvina and Pfaendtner (1995), Wu and Derber

Corresponding author address: Dr. Godelieve Deblonde, Data Assimilation and Satellite Meteorology Division, Atmospheric Environment Service, 2121 Trans-Canada Highway, Dorval, PQ H9P 1J3, Canada.
E-mail: godelieve.deblonde@ec.gc.ca

(1994), and Phalippou and Gérard (1996). These studies have demonstrated positive impacts on humidity analyses/forecasts. The study by Ledvina and Pfaendtner (1995) also showed an improvement of the forecast of precipitation in the Tropics. The evaluation method was, however, highly subjective. SSM/I TBs have been assimilated using the European Centre for Medium-Range Weather Forecasts (ECMWF) analysis/forecast system by Phalippou (1996). This technique is very computer intensive due to the complex calculations involved in the simulation of the oceanic surface emissivity at microwave frequencies (requires at least one-half of the total computation time). The computation of transmittances was based on the same technique as that used in Eyre (1991). The impact of assimilating a few SSM/I orbits showed that the technique was promising. Although the technique of assimilating SSM/I TB directly is by no means cost efficient, it offers better prospects in terms of reduced systematic TPW biases that are associated with regression methods.

In the Tropics, largely because of both a lack of adequate sampling of observations to determine the hydrological cycle and the complexities involved in modeling precipitation processes, numerical weather prediction (NWP) models tend to exhibit large TPW biases. NWP models such as the one employed in Ledvina and Pfaendtner (1995) that used the National Aeronautics and Space Administration Goddard Earth Observation System data assimilation system exhibit a dry bias in the Tropics. Large areas of biases were also observed in the National Centers for Environmental Prediction (NCEP) global NWP (Wu and Derber 1994). A dry bias was also found in the ECMWF NWP model (Phalippou and Gérard 1996). The assimilation of SSM/I TPW using these models was shown to reduce these biases in short- to medium-range forecasts.

Usually, in global analysis systems, the humidity analyses are univariate. The only way that changes in humidity will have an impact on the dynamical fields is through the first-guess field as it evolves during an assimilation cycle. As was shown in McNally and Vesperini (1996), assimilation of TB for High Resolution Infrared Sounder humidity channels 10, 11, and 12 did have a significant impact on the mean meridional humidity transport and the vertical velocity.

At the Canadian Meteorological Centre (CMC), humidity observations that are assimilated operationally consist of conventional observations and profiles of dewpoint depression (DPD) derived from Geostationary Observing Earth Satellite (GOES) radiances (Garand 1993; Garand and Hallé 1997). GOES-derived profiles of DPD have been assimilated operationally at CMC since 1993. The impact of assimilating these profiles of DPD on the CMC analyses/forecasts system was evaluated through comparison against the network of radiosondes. A more in-depth study of this impact is presented here since the main objective is to assess the impact on the operational analysis/forecast system of assimilating SSM/I-retrieved TPW. The 3D variational assimilation (3D-Var) system that became operational at CMC in June 1997 (Gauthier et al. 1996) was used in this study and the NWP model employed was the spectral finite element (SEF) model.

In section 2, a description of the techniques employed to derive the satellite retrievals of humidity (SRH) is given for both the GOES and SSM/I retrievals. Accuracy estimates of the retrievals derived from collocations with radiosondes are presented. A description of the 3D-Var system and the design of experiments is given in section 3. An impact assessment on the analysis/forecast system due to the assimilation of SRH is given in section 4. First, the evaluation of the assimilation of SSM/I TPW was performed using collocations with radiosondes, calculating geopotential anomaly correlations, and by simulating TIROS-N Operational Vertical Sounder (TOVS) TB for the control cases and the experiments. Second, the impacts on TPW, precipitation, and specific humidity are presented. Third, the impact on the Hadley cell circulation and mean meridional transport of humidity is investigated, and, finally, a comparison is done between the NCEP reanalyses (Kalnay et al. 1996) and the CMC analyses. Conclusions are presented in section 5.

2. Humidity observations and satellite retrievals

Humidity observations assimilated by the 3D-Var system at CMC consist of conventional observations (radiosonde and surface observations) and GOES retrievals of DPD. The retrievals of DPD are derived from *GOES-8* and *GOES-9* radiances using a system named Humsat (humidity from satellites). A description of the Humsat DPD retrieval procedure and the new humidity data source that consists of SSM/I retrievals of TPW follows.

a. Humsat profiles of dewpoint depression

The Humsat system produces profiles of DPD on a $1^\circ \times 1^\circ$ grid at pressure levels of 1000, 925, 850, 700, 500, 400, and 300 hPa over the *GOES-8* and *GOES-9* viewing areas (one satellite covers ~20% of the globe). The area covered by both satellites extends roughly between 60°S and 60°N latitude and 160°E and 30°W longitude. To compute the retrievals, three channels of full disk images are employed when available. These are the IR channel (10.5–12 μm), the visible channel (0.55–0.75 μm), and the water vapor channel (6.7 μm) whose weighting function peaks near 400 hPa. Up to three features are extracted (cloud-top pressure, cloud fraction, and mean-cloud albedo) using the IR and/or visible channels. Ancillary data such as the background (6-h forecast) temperature and SST analyses are used to extract these features, which are then identified with a cloud class. Subsequently, each cloud class is assigned a profile of DPD, which was determined a priori from

a large dataset of collocated radiosondes. In clear skies, profiles of DPD are based on climatology. Humidity above 600 hPa is improved upon using a derived linear relationship between DPD and the 6.7-μm channel TB. This linear relation was recently revised (Garand and Hallé 1997) in the context of the *GOES-8* and *GOES-9* satellites. A more stringent quality control of the DPD retrievals and refinements of the retrieval procedure are described in Deblonde et al. (1995).

In the current version of the 3D-Var system, horizontal error correlations for the observations are not included. Hence, the spacing of Humsat retrievals was increased from 100 km [in a prior optimal interpolation analysis system; Mitchell et al. (1993); Garand and Hallé (1997)] to 300 km. The data volume consists of about 10 000 profiles per 6-h period. Over land, Humsat DPDs are assimilated mainly above 600 hPa while over the oceans usually all levels below and including 300 hPa are assimilated.

Table 2 of Deblonde et al. (1995) lists collocation statistics between Humsat TPW and all radiosonde observations that were available. To compute Humsat TPW, Humsat DPD was first converted to specific humidity (q) using the 6-h temperature forecast. For a tropical dataset (mean TPW of 40 kg m^{-2}) the rmsd was 6.8 kg m^{-2}, which is larger than for the SSM/I TPW as is shown in the next section.

b. SSM/I total precipitable water retrievals

The Defense Military Satellite Project (DMSP) SSM/I instrument is located on board a polar-orbiting satellite and has four channels (19.35, 22.235, 37, and 85.0 GHz), three of which have dual polarization. The 22.235-GHz channel has only a vertical polarization and samples a relatively weak water vapor absorption line. The nominal resolution of the three lowest frequencies is 25 km and 12.5 km for the 85.5-Ghz channels. The SSM/I instrument is a conical scanner and has a swath width of ~1400 km. Considering the relatively low resolution at which the analyses of humidity are performed (section 3a), only every eighth scan and every eighth pixel of the remaining scans were kept. This corresponds to a resolution of ~200 km. About 2000 SSM/I pixels were used per 6-h assimilation period.

TPW was computed from the *F-13* satellite and the SSM/I TBs were obtained from Remote Sensing Systems (RSS) (Wentz 1993). The *F-13* TBs were intercalibrated with the *F-8* TB using a linear correction equation provided by RSS. A multiple regression relation was used to derive TPW from TB (Alishouse et al. 1990). A cubic polynomial correction developed by Petty (in Colton and Poe 1994) was applied to TPW. This correction accounts partially for the systematic overestimation of TPW for low values and underestimation at high values. This procedure to compute TPW is also currently used to produce TPW estimates operationally at the Fleet Numerical Meteorology and Oceanography Center (FNMOC). TPW can only be retrieved over the oceans (because the surface of the ocean has a much lower emissivity than land) and when precipitation is not present. The precipitation screen of Alishouse et al. (1990) was used, which is based on a linear combination of the 37-GHz horizontal and vertical polarization channels. In Deblonde and Wagneur (1997), it was shown that for October 1993 (*F-10* and *F-11* data), application of the precipitation screen lead to a rejection of 11% of potential retrievals.

TABLE 1. Statistics of collocations of *F-13* SSM/I TPW with collocated radiosondes (units are kg m^{-2}).

Period	N	Correlation	Rmsd	Mean raob	Mean satellite
Jan 1996	252	0.96	3.94	30.81	32.59
Jul 1996	300	0.95	5.55	40.32	44.26
Dec 1996	204	0.96	4.51	31.15	33.82

Table 1 and Fig. 1 show results of TPW collocations between SSM/I retrievals and all radiosondes available from small islands and ships for the months of January, July, and December 1996. The months of July and December 1996 correspond to the time window of the study in this paper. The collocation time and spatial window was $\pm$3 h and 50 km. The same collocation technique as described in Deblonde et and Wagneur (1997) was used. The rmsd for the month of July 1996 (Table 1) is larger than that cited in section 1. This is so because most of the observed TPW values vary between 40 and 60 kg m^{-2} (Fig. 1b) and give rise to a higher mean value. The higher the mean value of TPW, the higher one may expect the rmsd to be. To estimate the SMM/I TPW error variances, collocations with radiosondes for the entire year 1993 (*F-11* satellite) were used. Figure 2 illustrates the SSM/I TPW rmsd w.r.t. radiosondes as a function of TPW. Also shown is the error estimate as derived in Phalippou and Gérard (1996). This estimate was developed by fitting a line to SSM/I TPW rmsd w.r.t. radiosondes taken in Alishouse et al. (1990). Error estimates for *F-13* January, July, and December 1996 TPW also showed a similar behavior. A linear approximation to model the errors seems indeed to be adequate.

3. 3D-Var analysis system and design of experiments

a. 3D-Var analysis system

The 3D-Var system (Gauthier et al. 1996) employs the incremental approach. The analysis vector $\mathbf{x}^a$ is defined as follows:

$$\mathbf{x}^a = \mathbf{x}^b + \delta\mathbf{x}^a, \tag{1}$$

where $\mathbf{x}^b$ is the background state (6-h forecast) and $\delta\mathbf{x}^a$ is the analysis increment obtained by minimizing the following cost function:

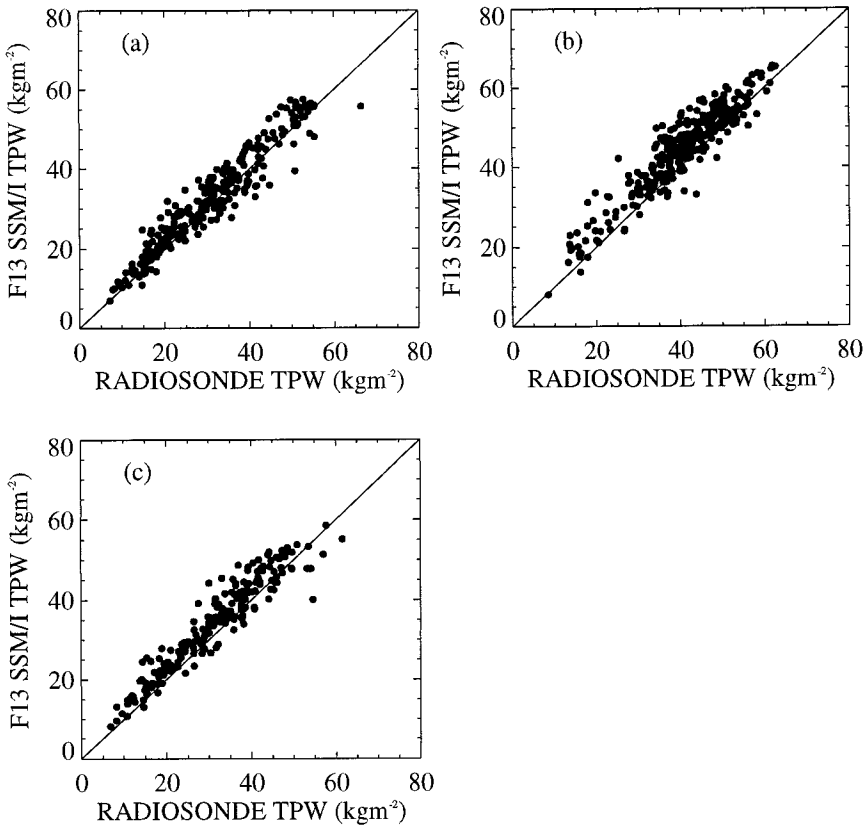

FIG. 1. Collocations of *F-13* SSM/I-retrieved TPW and radiosonde TPW: (a) Jan 1996, (b) Jul 1996, and (c) Dec 1996.

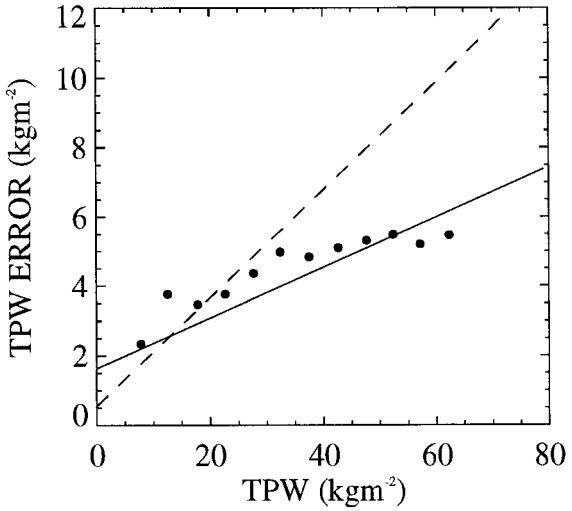

FIG. 2. SSM/I TPW error as a function of TPW. The solid line represents the curve taken from Phalippou and Gérard (1996). The circles represent *F-11* SSM/I TPW rmsd with respect to collocated radiosondes for the year 1993. TPW values were binned by 5 kg m^{-2}. The dashed line is a linear fit to the TPW background (6-h forecast) error SD for each point on the globe valid on 0000 UTC 19 Jul 1996.

$$J(\delta\mathbf{x}) = \frac{1}{2}\delta\mathbf{x}^{\mathrm{T}}\mathbf{B}^{-1}\delta\mathbf{x} + \frac{1}{2}(\mathbf{H}\delta\mathbf{x} - \mathbf{d})^{\mathrm{T}}\mathbf{R}^{-1}(\mathbf{H}\delta\mathbf{x} - \mathbf{d}), \quad (2)$$

where $\mathbf{B}$ is the covariance matrix of background errors, $\mathbf{R}$ is the covariance matrix of observation errors, and $\mathbf{H}$ is the linear approximation to the observation simulator operator H in the vicinity of $\mathbf{x}^b$. In addition, $\mathbf{d}$ is the innovation vector and is defined as

$$\mathbf{d} = \mathbf{y}^o - \mathbf{H}\mathbf{x}^b, \quad (3)$$

where $\mathbf{y}^o$ is the observation vector. The analysis increments are represented in spectral space in terms of the rotational and divergence components of the horizontal wind, the geopotential departure from geostrophy, and DPD. In the extratropics, the geopotential is related to the horizontal wind components by a constraint that imposes a local balance of geostrophy. The analysis is performed every 6 h in pressure coordinates at the 16 mandatory levels between 1000 and 10 hPa. The humidity analysis is univariate and the highest level for the humidity analysis is 300 hPa. Above 300 hPa, the humidity is extrapolated and is kept constant at the 300-hPa value. If the temperature decreases with height (i.e., under the tropopause), then it is the relative humidity that is kept constant. If the temperature increases with height (i.e., above the tropopause), then it is the specific

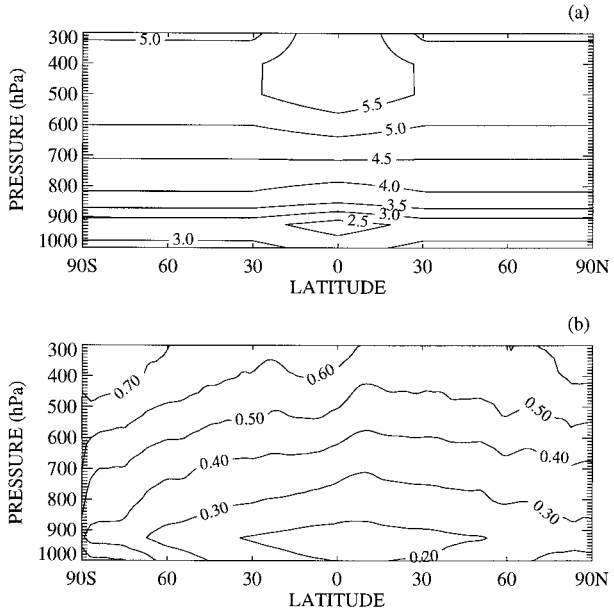

FIG. 3. Background error SD as a function of latitude and pressure for July. (a) Errors for DPD (K) and (b) errors for ln(q).

humidity that is kept constant. If the pressure is less than 100 hPa, then the minimum value of q is fixed at 2.5×10^{-6} kg kg^{-1}.

To accommodate the assimilation of TPW in the 3D-Var, the humidity variable DPD was replaced with the natural logarithm of specific humidity hereafter referred to as ln(q). The reason that ln(q) was chosen rather than q is because negative specific humidities are impossible by construction and the dynamic range of ln(q) is considerably smaller than that of q. The background error covariance matrices for ln(q) were computed from those of DPD. Figure 3 illustrates the standard deviation (SD) of the background error for DPD and ln(q). One may note a stronger temperature dependence for the ln(q) background error SD. Because the horizontal error correlations for ln(q) were not available, it was simply assumed that they were equal to those of DPD.

Due to the choice of the variable ln(q) instead of q, the simulator operator for TPW is no longer linear. To assimilate SSM/I TPW, a humidity term was simply added to the rhs of Eq. (2) defined as follows:

$$\frac{1}{2}\{\mathrm{TPW}[\ln(q)] - \mathrm{TPW}_{\mathrm{SSM/I}}\}^{\mathrm{T}} O^{-1} \times \{\mathrm{TPW}[\ln(q)] - \mathrm{TPW}_{\mathrm{SSM/I}}\}, \quad (4)$$

where TPW[ln(q)] is defined as

$$\mathrm{TPW}[\ln(q)] = \frac{1}{g}\int_{P_{\mathrm{top}}}^{P_{\mathrm{surf}}} \exp[\ln(q)]\, dP \quad (5)$$

and O is the SSM/I TPW error variance. Since the surface pressure is not analyzed by the 3D-Var system, the surface pressure of the background field was used to compute TPW. To compare the magnitude of the background error SD of TPW with the SSM/I TPW error, the background error SD for TPW was calculated following Deblonde et al. (1995) for a 6-h forecast at each point on the globe. A linear regression of the background error SD at all the points was calculated and is illustrated in Fig. 2 along with the SSM/I TPW errors. The background field error SD is considerably higher than that for the SSM/I TPW at large values of TPW. At low values of TPW the contrary holds.

The CMC global operational SEF model (Ritchie and Beaudouin 1994) is based on the primitive equations. It uses a spectral representation (triangular truncation at spherical harmonic 199: T199) in the horizontal and linear finite elements in the vertical (21 sigma levels). The physical parameterizations used by the model (Canadian Meteorological Centre 1993) include shallow convection, and large-scale and convective precipitation (Kuo-type moist convection). Cloud water is computed diagnostically.

The steps involved in the analysis cycle are as follows: 1) The innovation term **d** is calculated using the full resolution background field (T199), 2) the analysis increment $\delta\mathbf{x}^a$ is computed at a resolution of T108 (corresponding to a resolution of ~180 km at the equator), and 3) the analysis increments are then transformed to physical space. To use the analysis to start a forecast, the increments are interpolated to the model levels, and geopotential increments are converted to temperature increments using the hydrostatic relation. The converted increments are then added to the background field to obtain the analysis in model coordinates.

The adiabatic nonlinear normal mode initialization used to initialize the analyses was shown to affect the Hadley circulation only slightly (Fillion et al. 1995). This was reevaluated in the context of this study and is discussed in section 4b.

b. Experimental design

To estimate the impact of the assimilation of humidity retrievals from Humsat and SSM/I, a set of control cases and experiments was set up. Assimilation cycles were performed for the months of July and December 1996. In order to allow for the analysis to adjust to its new setup, the assimilation for the control cases was started one week before that of the experiments. The control experiments only assimilated conventional humidity observations. Assimilation experiments consisted of adding Humsat DPD retrievals only, SSM/I TPW retrievals only, and both SSM/I and Humsat retrievals to the conventional observations. To assimilate Humsat DPD, background temperature profiles were used to convert DPD to ln(q). For the first two weeks of the months and for the control and experiment cases, 5-day forecasts were launched once a day at 0000 UTC. For the remainder of the months, 2-day forecasts only were per-

TABLE 2. Naming convention for the control cases and experiments.

Name	Control/expt	Humidity data assimilated
ln(q):C	Control	Conv**
ln(q):CH*	Experiment	Conv + humsat DPD profiles
ln(q):CS	Experiment	Conv + SSM/I TPW
ln(q):CSH	Experiment	Conv + SSM/I TPW + humsat DPD profiles

* The ln(q):CH assimilation cycle was only run for the first two weeks of each month.
** Conv = radiosondes and surface observations.

formed. The naming convention for the control cases and experiments is presented in Table 2.

4. Analysis/forecast impact assessment due to the assimilation of satellite-retrieved humidity

a. Evaluation of assimilation of SSM/I TPW

Because of the lack of conventional observations over the oceans, the task of showing that SSM/I TPW improved the analyses/forecasts comprised several techniques discussed below.

1) COLLOCATIONS WITH RADIOSONDES

To evaluate the assimilation of SSM/I TPW, a subset of the worldwide radiosonde network (which is used for verification purposes at CMC) was selected because SSM/I TPW were assimilated only over the oceans and at least 100 km away from land. The subset consisted of stations that were located on islands surrounded by water. Figures 4a and 4b illustrate the bias and SD for ln(q) in the Tropics. There is an improvement in both the analyses and the 6-h forecast for levels 700 hPa and above. The curves of geopotential (not shown) remained the same and the winds improved somewhat (Figs. 4c–f). Figure 5 illustrates the same statistics for the Southern Hemisphere (SH) extratropics and shows mainly a reduction in the bias of ln(q). There is also a reduction in the bias for the geopotential (Figs. 5a and 5b) and the winds remained unchanged (not shown). The impact for the winter case was also positive but was not as large. The reason why this is so will be discussed in section 4b(1). It should be emphasized that the radiosondes used for the validation were also assimilated.

2) GEOPOTENTIAL ANOMALY CORRELATIONS

Geopotential anomaly correlations were computed for 5-day forecasts for the period 6–15 July 1996 (one forecast per day, launched at 0000 UTC). The anomaly correlations (Table 3) were evaluated for three latitude bands: 20°–90°N, 20°S–20°N, and 20°–90°S. No changes were observed in the 20°N–90° latitude band. For the other latitude bands, the anomaly correlation increased by 1%–2% starting with the day 3 forecast in the Tropics and day 4 forecast in the SH extratropics.

3) TOVS BRIGHTNESS TEMPERATURE SIMULATIONS

National Oceanic and Atmospheric Administration Satellite-12 (*NOAA-12*) TOVS TB clear-sky simulations for HIRS channels 10, 11, and 12 (known as the TOVS water vapor channels) using background fields over the oceans for the first 15 days of July 1996 (at 0000 and 1200 UTC) were compared with observed TBs obtained from the National Environmental Satellite, Data and Information System. The TBs were computed with the recently developed fast physical radiative transfer code (L. Garand, D. S. Turner, C. Chouinard, and J. Hallé 1998, personal communication). Because only 0000 and 1200 UTC background fields in model coordinates were saved, there was a large gap in the coverage in the middle of the Pacific Ocean.

Table 4 lists the statistics for both the ln(q):C and ln(q):CS experiments. A negative (positive) bias in Table 4 indicates that on average the forecast is moister (drier) than the verifying analysis. Simply stated, addition of humidity to an atmosphere results in the weighting function peaking higher where temperatures are colder. In all regions and for all channels considered, the SD is slightly smaller as a result of assimilating SSM/I TPW. North of 30°S, the bias is reduced for channel 10 but is increased for channels 11 and 12. The midlatitude SH results show both a reduced bias and SD for channels 11 and 12, whereas for channel 10 only the SD is reduced.

Thus, the first two techniques of evaluation indicate an improvement due to the assimilation of SSM/I TPW on the analysis/forecast system. These improvements are small but are in the right direction. Since there was a small reduction in SD between TOVS observations and simulations, the last technique also showed an improvement as a result of assimilating SSM/I TPW.

b. Impact on TPW, precipitation, and specific humidity

1) TOTAL PRECIPITABLE WATER

TPW for the ln(q):C analyses was compared with the SSM/I TPW climatology. The SSM/I TPW climatology was obtained by computing the time average of the full resolution SSM/I TPW dataset using a straightforward averaging and binning technique on a $1° \times 1°$ grid. The statistics are presented in Table 5. The high correlation and relatively low rmsd indicate that on a monthly timescale, the control-case analyzed TPW is already in good agreement with the SSM/I TPW. A lower rmsd for the winter analyses also shows that these analyses are in better agreement with the SSM/I TPW. This could explain why the impact due to the assimilation of SSM/I TPW shown with the radiosonde collocation study dis-

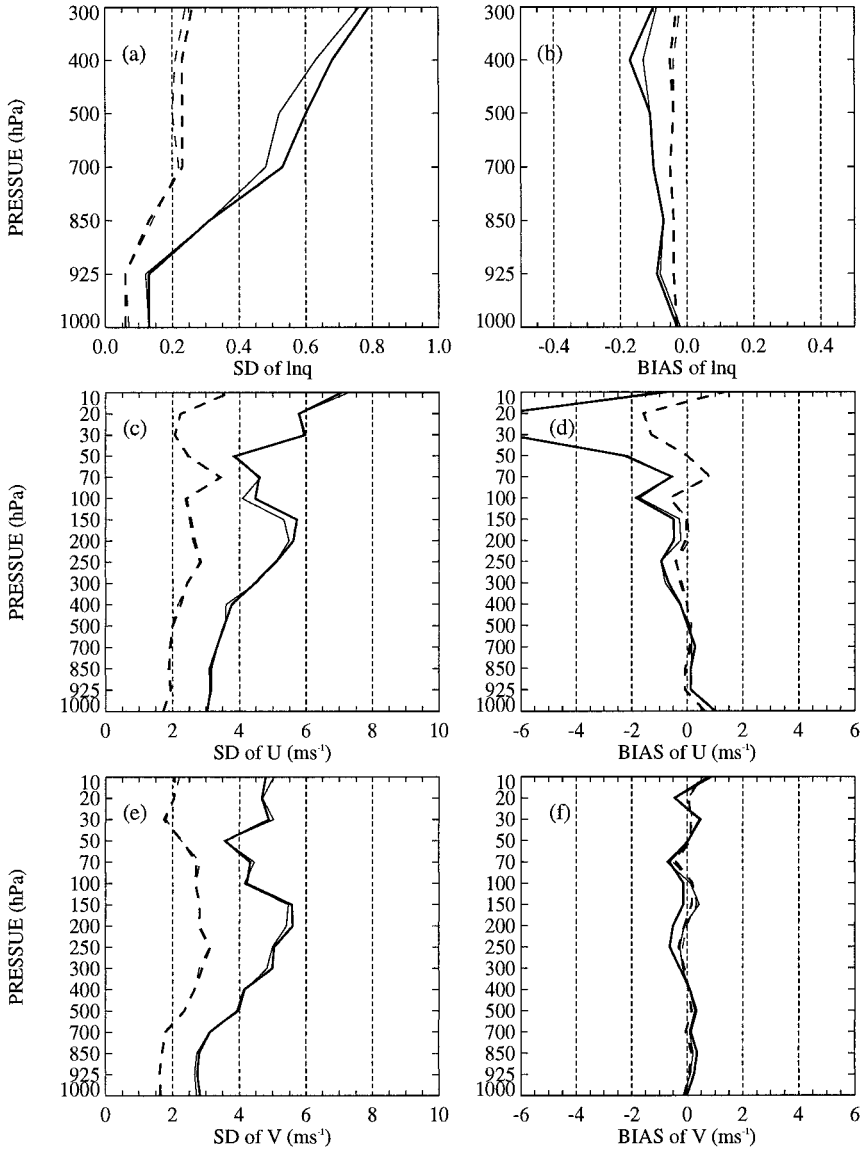

FIG. 4. Verification statistics over the Tropics zone (from 20°S to 20°N) for 1–31 Jul 1996 and for radiosonde stations launched from islands (total of 18 stations). Solid lines represent observation minus forecast statistics for ln(q):C (thick lines) and ln(q):CS (thin lines). Dashed lines represent observation minus analysis statistics for ln(q):C (thick lines) and ln(q):CS (thin lines). The symbols U and V represent zonal and meridional velocity, respectively.

cussed in section 4a(1) was not as large for the winter case compared with the summer case. For both the December and July cases, the analyses over the oceans are more humid than the SSM/I TPW retrievals.

The SSM/I TPW climatology was also used to find out whether the assimilation of Humsat DPD profiles improved the analyses. Statistics are presented in Table 6. The assimilation of Humsat DPD profiles reduced the rmsd of the analyses w.r.t. SSM/I TPW climatology for the July case but not for the winter case. It should be noted that the impact of assimilating Humsat data is somewhat limited in these statistics since the statistics are global and Humsat DPD retrievals only cover 40% of the globe.

The impact of assimilating SRH on the analyzed TPW for the first 15 days of July 1996 and December 1996 is illustrated in Figs. 6 and Fig. 7, respectively. These figures illustrate differences between the ln(q):C case and each of the experiments (Table 2). The magnitude of the differences for experiments ln(q):CS and ln(q):CH is similar. For the summer case (Fig. 6), an increase of humidity in the North Atlantic Ocean and in the Northern Hemisphere (NH) central Pacific Ocean ITCZ (180°–100°W longitude) appears both in the ln(q):CS

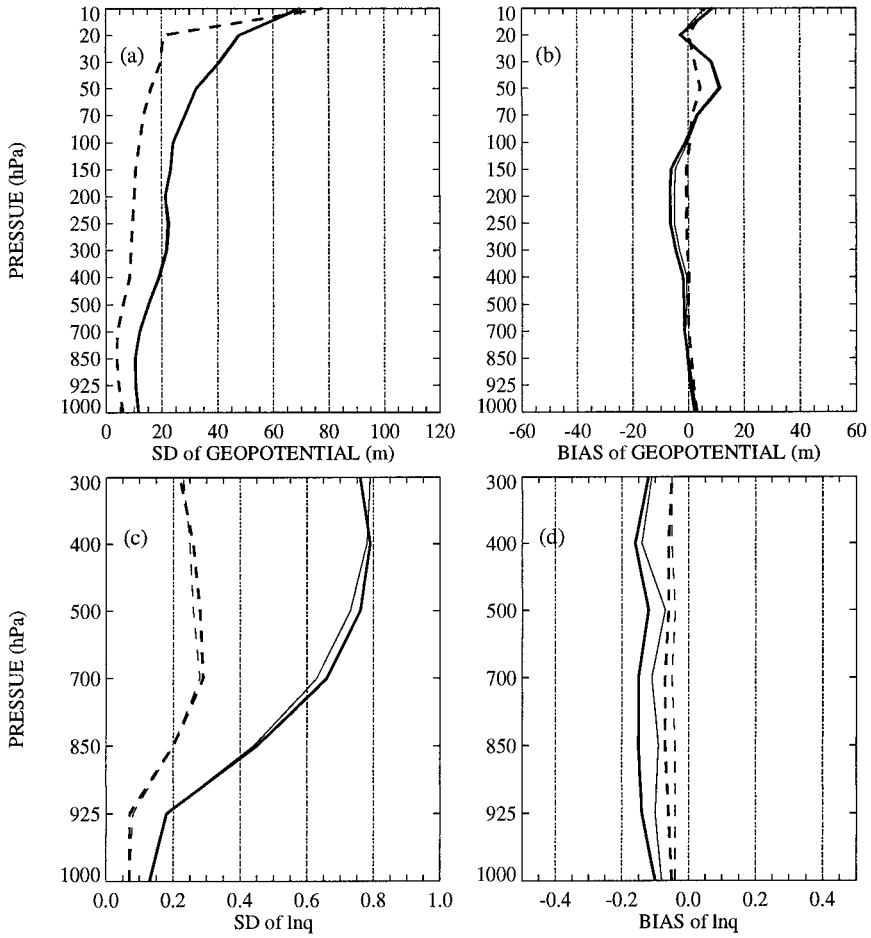

FIG. 5. Same as in Fig. 4 but for the Southern Hemisphere extratropical zone (from 90° to 20°S). The geopotential is illustrated here instead of zonal meridional velocity. Total number of radiosonde stations used for collocation was 12.

and ln(q):CH experiments. The latter area of humidity increase enhances the zonal distribution of the ITCZ TPW in agreement with the SSM/I TPW climatology. A large decrease in humidity for both experiments (ln(q):CS and ln(q):CH) also appears in the South Pacific convergence zone (SPCZ) although the regions of maximum change are slightly shifted w.r.t. each other. For the winter case (Figs. 7b and 7c), due to the assimilation of SRH, a similar increase in humidity appears again in the central Pacific ITCZ and in the North Atlantic Ocean between 0° and 20°N. TPW for the ln(q):CS experiment (Fig. 7b) is decreased off the east coast of Africa (southeastern monsoon). This points to a problem with the simulation of the southeastern monsoon. The ITCZ also reaches farther south over the ocean south of eastern Africa.

Striking differences between the ln(q):CS and ln(q):CH experiments occur east and west of South America along the equator (larger difference for winter case) and in the Pacific Ocean off the west coast of South America (larger difference for the summer case). In the latter area, decks of stratocumulus clouds are prevalent. In this region, Humsat overestimates the humidity considerably. Although, the cloud structures are readily identifiable with Humsat, radiosondes in such cloud structures are not available in order to ''calibrate'' these retrievals and therefore the retrievals turn out to be largely biased (see also Deblonde et al. 1997). A large overestimation of humidity in this region was also found to be present when TOVS humidity profiles (by layers) were assimilated (e.g., Liu et al. 1992). A humidity bias of the same sign was also obtained when TOVS radiances were assimilated (McNally and Vesperini 1996).

The drier zones of subsidence east and west of South America along the equator line are too dry for the ln(q):CH experiment (Fig. 7c). Since the Humsat technique is based on cloud classification, it is difficult to assign humidity in clear skies. A climatology value is used and so a bias can be easily introduced. The fact that these areas had a low cloud fraction was verified with the cloud fraction climatology (not shown) obtained with the Humsat system (section 2a).

TABLE 3. Geopotential anomaly correlations per latitude band for 6–15 Jul 1996. Different correlations are in bold.

		Latitude band			
		20°S–20°N		20°–90°S	
Expt		ln(q):C	ln(q):CS	ln(q):C	ln(q):CS
Pressure level: 850 hPa					
Forecast time (h)	0	0.98	0.98	1.00	1.00
	24	0.90	0.90	0.98	0.98
	48	0.86	0.86	0.94	0.94
	72	0.79	**0.80**	0.87	0.87
	96	0.74	**0.75**	0.79	**0.80**
	120	0.69	**0.71**	0.68	**0.70**
Pressure level: 700 hPa					
Forecast time (h)	0	0.97	0.97	1.00	1.00
	24	0.92	**0.91**	0.98	0.98
	48	0.87	0.87	0.94	0.94
	72	0.80	**0.81**	0.87	0.87
	96	0.75	**0.76**	0.79	**0.81**
	120	0.69	**0.70**	0.69	**0.70**
Pressure level: 500 hPa					
Forecast time (h)	0	0.98	0.98	1.00	1.00
	24	0.93	0.93	0.99	0.99
	48	0.88	0.88	0.95	0.95
	72	0.82	0.82	0.88	0.88
	96	0.78	0.78	0.80	**0.81**
	120	0.72	**0.74**	0.70	**0.71**

SSM/I TPW in the experiments is assimilated strongly (i.e., where SSM/I TPW was assimilated, the fit of the analysis to the SSM/I TPW was very good). This is illustrated by the large reduction in rmsd as a result of assimilating these data (Table 5). Differences between the monthly mean TPW of the ln(q):CS experiment and SSM/I TPW climatology (not shown) confirmed this conclusion. It appears that the Humsat data is also assimilated strongly since changes as a result of the assimilation are of the same order of magnitude as for the SSM/I data assimilation. In the case of SSM/I TPW assimilation (experimental study and not operational), the fact that the assimilation is strong is not necessarily a detriment, since a maximum impact study is then performed. The strong assimilation of SSM/I TPW data is due to a combination of two factors: 1) the relative weight of the observation versus background error covariances and 2) a high observation data volume [compared to the actual resolution of the minimization of the cost function Eq. (2)] and omission of horizontal correlations in the observations errors (which are not representable in the current version of the 3D-Var). The first factor was tested by changing the relative weight of the observation versus background error SD by a factor of 2. This change only had a small impact on the analyses. When the volume of data assimilated was reduced further, a larger control over the impact of the ratio of errors was found. When both sources of SRH were assimilated (Figs. 6d and 7d), a TPW increment was obtained such that both sets had weights of similar magnitude. Thus, neither satellite dataset dominated strongly over the other.

Figures 8 and 9 summarize the differences in the zonal averages of TPW as a function of latitude w.r.t. the control case as a result of assimilating SRH. The analyses were averaged over the first 15 days of July 1996 (Fig. 8) and December 1996 (Fig. 9). In the ITCZ north of the equator the result of assimilating SSM/I TPW and/or Humsat DPD is to increase the humidity. For both the summer and winter cases there is a decrease in humidity in the SH midlatitudes. For the winter case, both the SH and NH midlatitudes are dried out as a

TABLE 4. TOVS statistics of TB differences between observations and simulations over clear-sky oceans for *NOAA-12*: 1–15 Jul 1996 at 0000 and 1200 UTC (units are in kelvins).

(a) No. of samples for each experiment

	Latitude bands		
Expt	60°–30°S	30°S–30°N	30°–60°N
ln(q):C	12 543	39 486	7610
ln(q):CS	12 521	39 818	7625

(b) TB differences (observation-simulation) and SD of differences

		Latitude bands					
		60°–30°S		30°S–30°N		30°–60°N	
Expt	Channel	Mean	SD	Mean	SD	Mean	SD
ln(q):C	10	−1.27	1.19	−0.65	1.39	−0.82	1.46
ln(q):CS	10	−1.36	1.16	−0.54	1.26	−0.72	1.41
ln(q):C	11	2.32	2.76	2.31	3.21	1.41	2.48
ln(q):CS	11	2.14	2.67	2.44	3.03	1.64	2.41
ln(q):C	12	1.40	3.66	1.93	4.26	0.78	3.33
ln(q):CS	12	1.30	3.59	1.97	4.13	0.89	3.30

TABLE 5. Statistics of SSM/I TPW climatology (oceans only) compared with analyses with and without the assimilation of SSM/I TPW (units are kg m^{-2}).

Expt	Correlation	Rmsd	Mean analysis	Mean satellite
SSM/I TPW climatology: Jul 1996				
ln(q):C	0.98	2.98	27.83	27.48
ln(q):CS	1.00	1.16	27.75	27.48
SSM/I TPW climatology: Dec 1996				
ln(q):C	0.98	2.64	27.90	26.98
ln(q):CS	1.00	1.34	27.50	26.98

TABLE 6. Statistics of SSM/I TPW climatology (oceans only) compared with analyses with and without the assimilation of Humsat DPD retrievals (units are kg m^{-2}).

Expt	Correlation	Rmsd	Mean analysis	Mean satellite
SSM/I TPW climatology: 1–15 Jul 1996				
ln(q):C	0.98	3.29	27.56	27.20
ln(q):CH	0.98	2.90	27.86	27.20
SSM/I TPW climatology: 1–15 Dec 1996				
ln(q):C	0.98	2.98	27.65	26.98
ln(q):CH	0.98	3.00	27.71	26.98

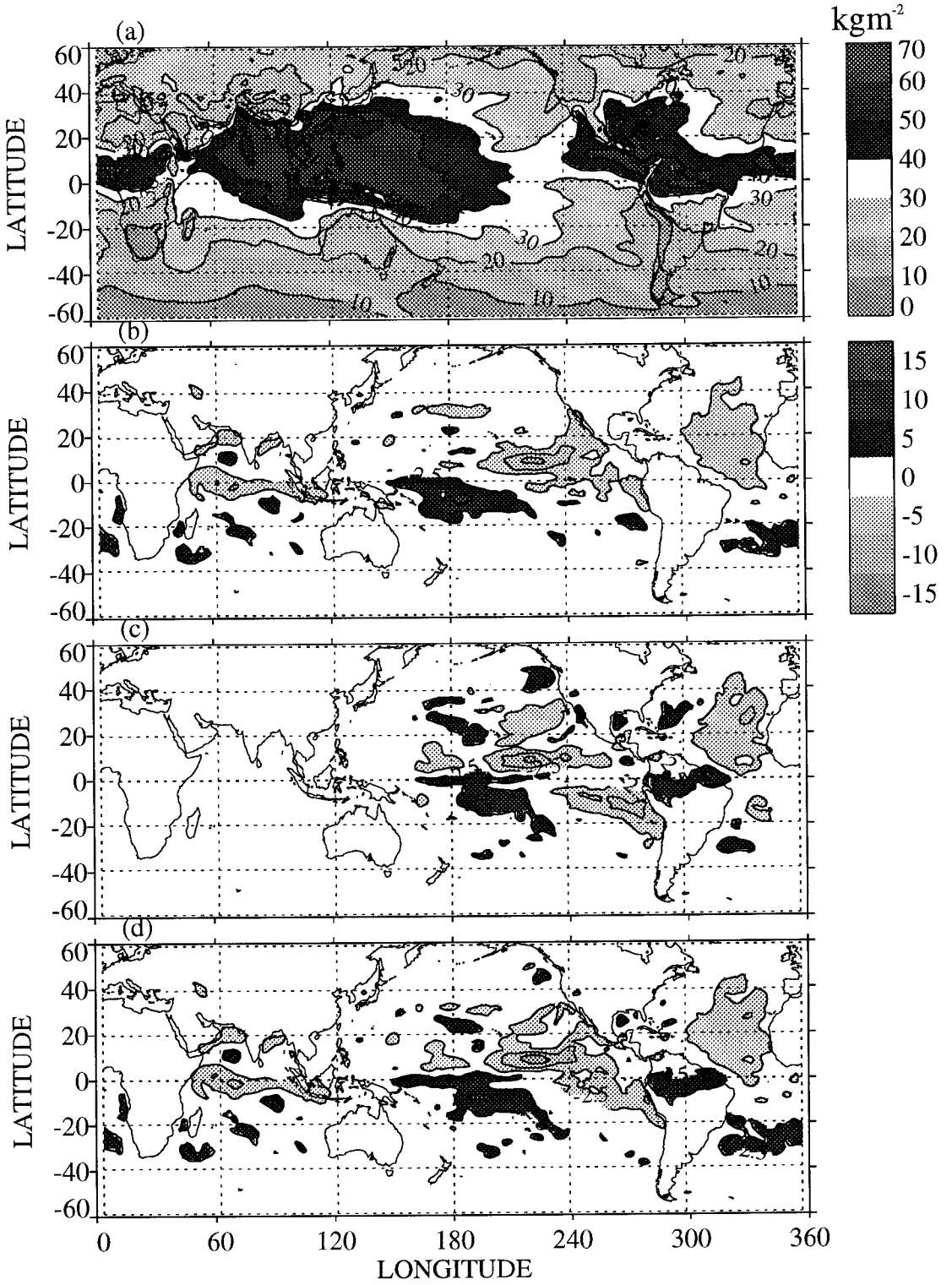

FIG. 6. Analyzed TPW averaged every 6 h from 1 to 15 Jul 1996: (a) ln(q):C, (b) ln(q):C − ln(q):CS, (c) ln(q):C − ln(q):CH, and (d) ln(q):C − ln(q):CSH.

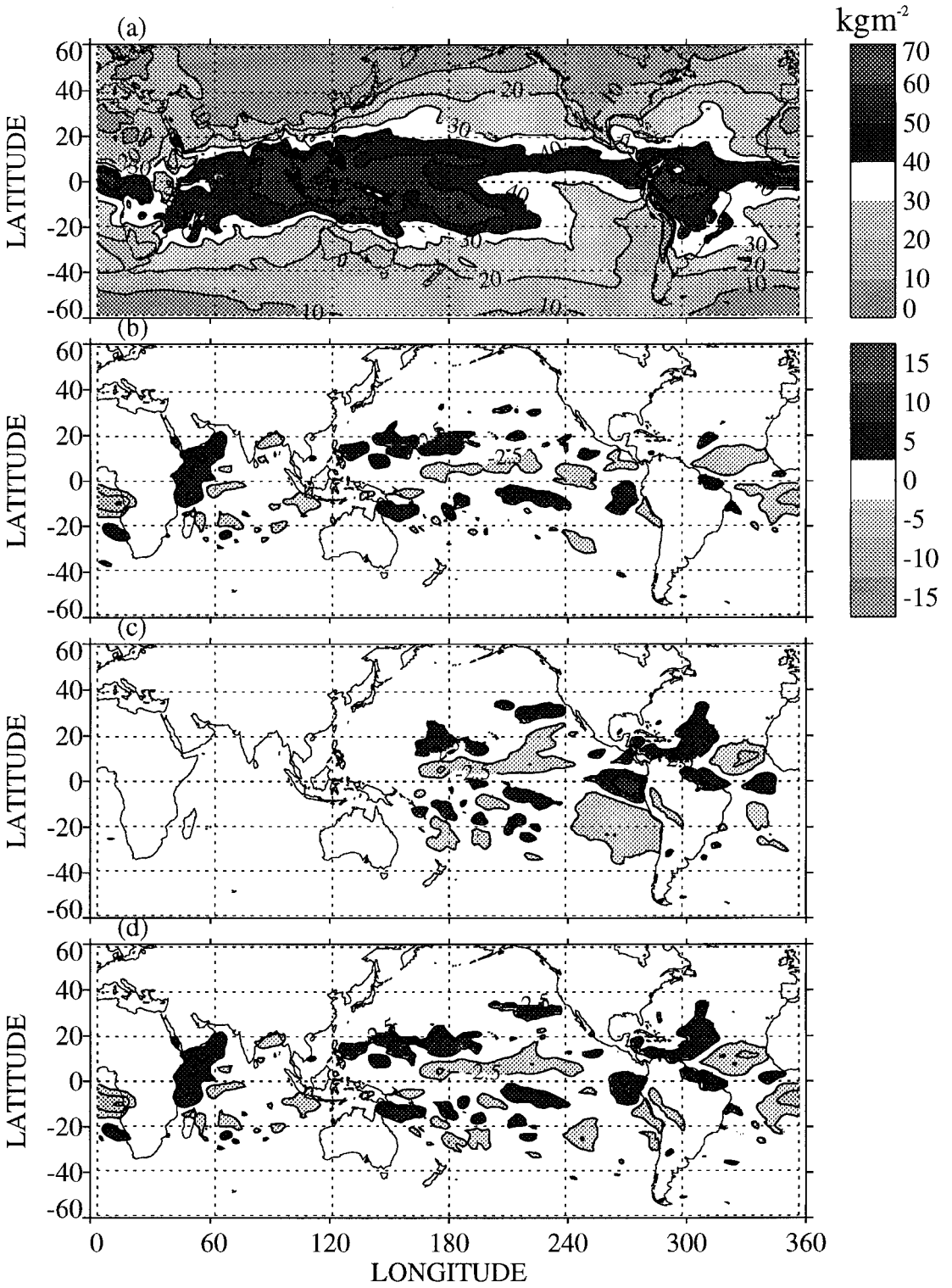

FIG. 7. Same as in Fig. 6 but for 1–15 Dec 1996.

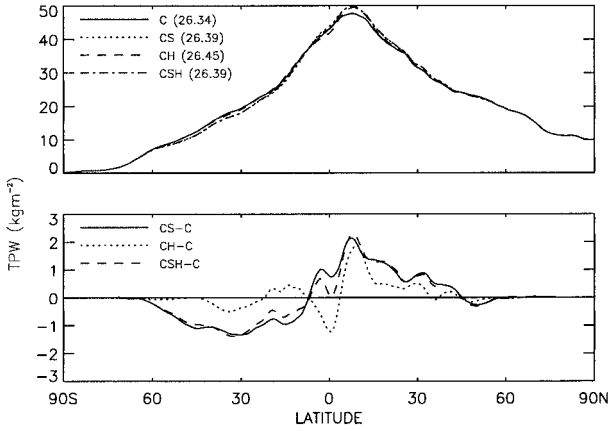

FIG. 8. (top) Zonally averaged analyzed TPW every 6 h from 1 to 15 Jul 1996; ln(q) was dropped from the experiment names (see Table 2). The numbers in parentheses represent global averages. (bottom). Same as in top panel but for differences between experiments.

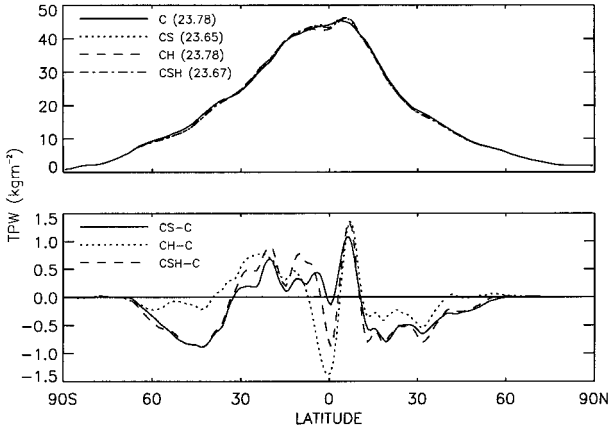

FIG. 9. Same as in Fig. 8 but for 1–15 Dec 1996.

result of the assimilation. The difference between the temporal average of the ln(q):C background fields and analyses were computed for 1–15 July 1996 (not shown). In the SH extratropics, conventional observations also indicated that the forecast is too moist, which is in agreement with the correction required by the assimilation of SRH. The maximum and minimum zonally averaged differences between the ln(q):CS and the ln(q):C experiments are 2.15 and -1.3 kg m^{-2} for the July case and 1.1 and -0.9 kg m^{-2} for the December case. Thus as was expected, the disagreement between the ln(q):CS and the ln(q):C experiments is smaller in winter. As was shown before, the winter TPW analyses of the control case were already closer to the SSM/I TPW climatology.

The impact of assimilating SRH on the 5-day forecasts (for the first 15 days in July 1996) was evaluated by collocating the forecasts with SSM/I TPW retrievals, Rmsd between the collocated forecasts and SSM/I TPW for different latitudinal bands on the globe are illustrated in Fig. 10. The impact of assimilating SSM/I TPW lasts for about 48 h in the Tropics and around 24 h in the midlatitudes. In the region 0°–20°N, a small impact lasts for 5 days. The only latitudinal band where Humsat DPD retrievals improved the forecasts according to this impact test was in the 0°–20°N latitudinal band where the ITCZ is found. Biases were also computed (not shown). As was discussed above, the SEF model has a wet bias in the SH midlatitudes and a dry bias in the ITCZ. After 6 h of forecast, the wet bias in the SH midlatitudes for the ln(q):CS forecast was ½ that of the ln(q):C forecast. In the ITCZ, the dry bias for the ln(q):CS forecast was ⅓ that of the ln(q):C forecast.

2) PRECIPITATION

It may be expected that precipitation will increase in geographical areas where the humidity is increased in the analyses provided the increase in humidity is large enough to trigger or significantly enhance precipitation processes. Verifying forecast precipitation is difficult because the error estimate observed precipitation is high, particularly over the oceans (e.g., Legates 1994; Huffman et al. 1997). The assimilation cycles in this study were purposely executed over a period of a month in order to compare the background and longer-range precipitation forecasts with monthly precipitation climatologies (e.g., Huffman et al. 1997).

NWP models are generally known to have a precipitation spinup or spindown. In the SEF model, there is a spinup. The spinup is measured here as the difference in global precipitation rate between the 6–0-h forecast and the 36–12-h forecast. For July 1996, the 6–0-h global precipitation rate is 3.23 and is 3.59 mm day^{-1} for

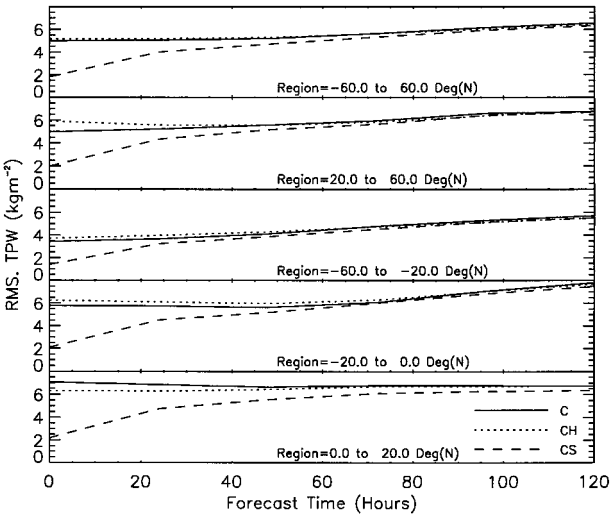

FIG. 10. TPW observation minus forecast rmsd as a function of forecast time for experiments ln(q):C, ln(q):CH, and ln(q):CS for different regions over the globe (1–15 Jul 1996, forecasts were started every 24 h at 0000 UTC). The observations are for the *F-13* SSM/I TPW at the same resolution as those that were assimilated; ln(q) was dropped from the experiment names (see Table 2).

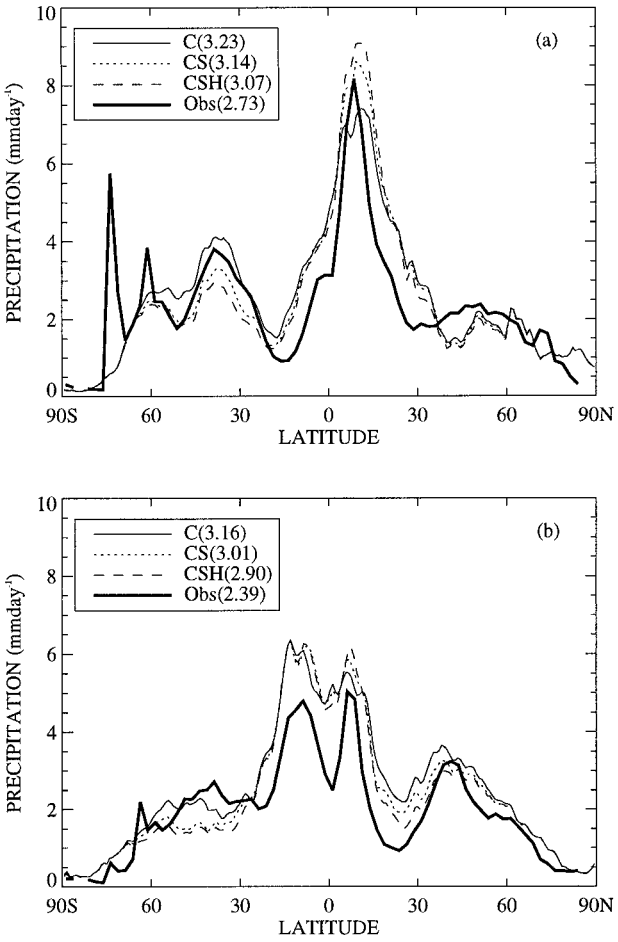

FIG. 11. Zonally averaged (6–0 h) precipitation rate for (a) Jul 1996 and (b) Dec 1996; ln(q) was dropped from the experiment names (see Table 2). Obs in the legend indicates observations from Huffman et al. (1997) for the satellite–gauge dataset. Numbers in parentheses in the legends represent the globally averaged precipitation rate.

the 36–12-h forecast. Often, the 36–12-h precipitation rate is considered to be representative of the NWP models because the spinup or spindown of the model should have settled down (Arpe 1991). The global precipitation rate observed for July 1996 on a 2.5° × 2.5° grid (Huffman et al. 1997) using the satellite–gauge technique is 2.73 mm day^{-1} and is 3.0 mm day^{-1} using the satellite-composite technique. The considerably higher 36–12-h SEF model forecast global precipitation rate suggests that the SEF model has a hydrological cycle that is too active. In an experiment where no humidity data at all were assimilated, the 6–0-h precipitation rate was even somewhat higher than for the ln(q):C case indicating that conventional observations of humidity act to reduce the global precipitation rate.

The zonally averaged background precipitation rates (6–0 h) for July and December 1996 for various experiments and observations (Huffman et al. 1997) are illustrated in Fig. 11. A striking feature for both months is that the peak of the ITCZ–SPCZ precipitation is much wider for the forecasts. The SEF model underestimates the size of the area where large-scale subsidence occurs. The width of the peak is reduced somewhat by the assimilation of SRH. For the July case, the precipitation at the peak value of the ITCZ is increased considerably as a result of assimilating SRH. Thus, the spinup of the peak value of the ITCZ will start from a higher value. In the SH midlatitudes and for both months, the precipitation is reduced considerably as a result of assimilating SRH, which appears to be in disagreement with the observations. However, according to the scattergrams of SSM/I TPW versus radiosonde TPW (Fig. 1), SSM/I TPW has a positive bias w.r.t. radiosonde TPW for values typically found in the SH midlatitudes (10–35 kg m^{-2}; see Figs. 8 and 9, top panels). This would correctly justify the decrease in humidity. For the winter case, the reduction of precipitation in the NH midlatitudes is in closer agreement with the observations. Precipitation in the NH subsidence zone is decreased, which results in a better agreement with the observations. For both months, assimilating SSM/I TPW decreases the global precipitation rate, which tends to decrease the wet bias of the SEF model.

Figure 12 illustrates precipitation rates averaged from 1 to 15 July 1996 for the control cases versus the experiments. As a result of assimilating SRH, the precipitation rate in the ITCZ in the eastern Pacific is more zonal, which is in better agreement with the observations (Huffman et al. 1997). Although Figs. 6 and 7 showed that the changes in TPW were of comparable magnitude as a result of assimilating either Humsat DPD or SSM/I TPW, the corresponding differences in precipitation are considerably larger in the ln(q):CH experiment (Fig. 12c) than for the ln(q):CS experiment (Fig. 12b). The same situation occurs for the winter case (not shown). An explanation for these differences is given in the next section.

3) SPECIFIC HUMIDITY

The reason that the precipitation difference between the ln(q):C and the ln(q):CH experiments is larger than that between the ln(q):C and the ln(q):CS experiments may be explained with the help of Fig. 13, which shows the difference in zonally averaged specific humidity over the eastern Pacific Ocean area extending from 180° to 100°W. For the ln(q):CH, one may notice that there is a strong drying out at the levels of 925–850 hPa in the large-scale subsidence area (0°–30°S) and in particular above the equator. There is also a large increase in humidity in the ITCZ (~10°N) from levels 850 to 500 hPa. This strong drying out in the subsidence zone and further humidification in the ITCZ strengthens the Hadley cell considerably (discussed further in the next section) and stimulates convection and hence increases precipitation. The strength of the Hadley cell circulation was also increased considerably for the winter case.

For the experiment ln(q):CH (Fig. 12), intense regions

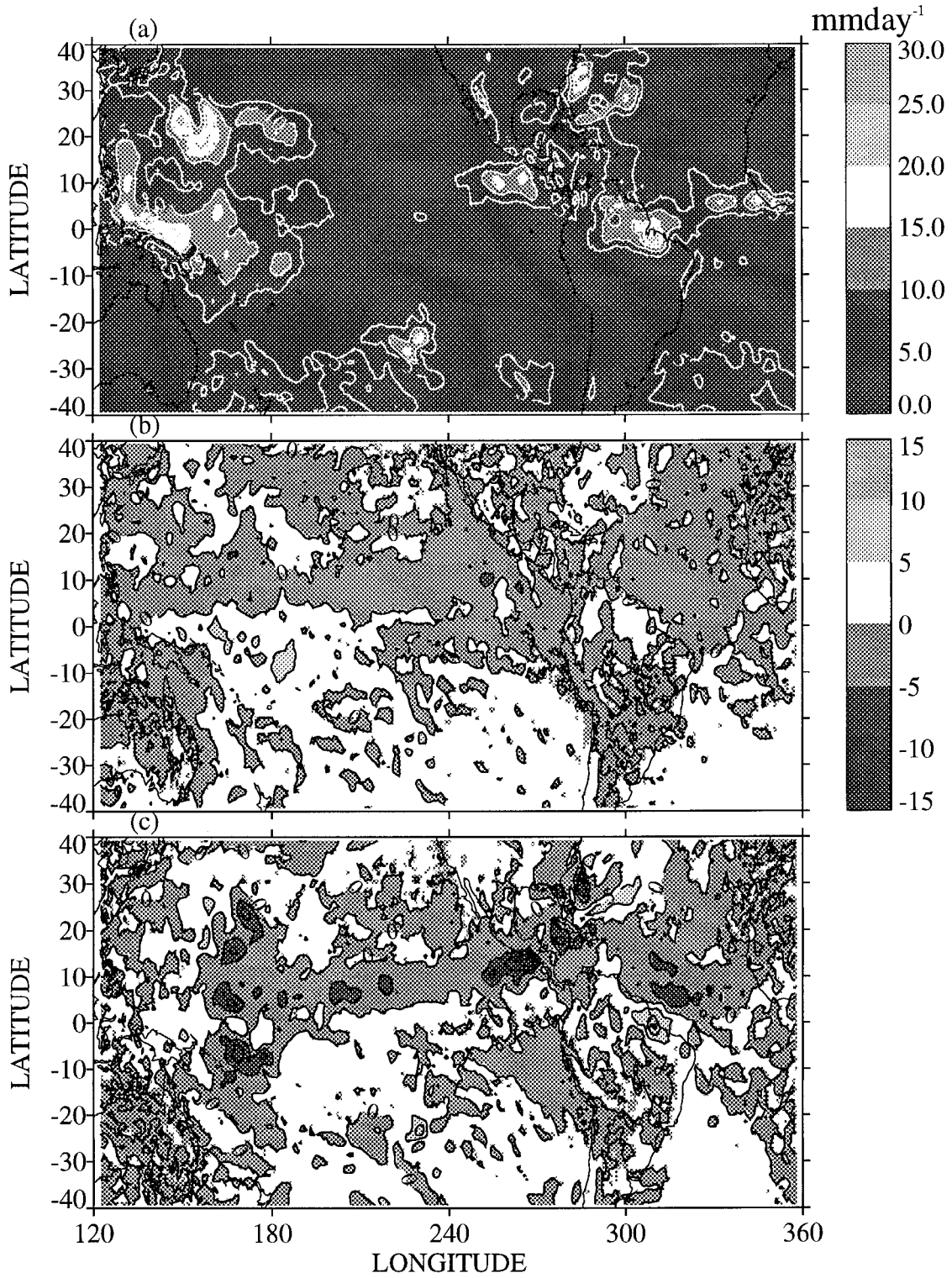

FIG. 12. Impact of assimilating SRH on the precipitation rate (6–0 h) for 1–15 Jul 1996: (a) ln(q):C (contour lines are in white and the interval is 5 mm day^{-1}), (b) ln(q):C − ln(q):CS, and (c) ln(q):C − ln(q):CH.

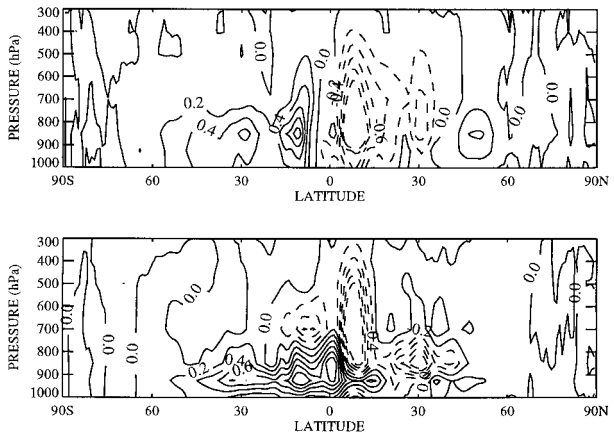

FIG. 13. Impact of assimilating SRH on analyzed specific humidity over the east Pacific Ocean region (180°–100°W) for 1–15 Jul 1996: (top) ln(q):C − ln(q):CS, (bottom) ln(q):C − ln(q):CH. Units are in g kg^{-1}.Dashed values are negative.

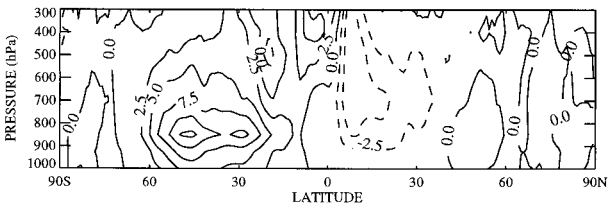

FIG. 14. Impact of assimilating SSM/I TPW on analyzed ln(q) over the globe for Jul 1996. Difference of ln(q):C minus ln(q):CS experiments multiplied by 100. These differences are equivalent to relative changes of specific humidity (%) provided that the values are less than 10%.

of precipitation appear in the western Pacific warm pool (along the meridian of ~165°W) that were weaker for the control case and even weaker or absent in the climatology for July 1996 (Huffman et al. 1997). This behavior may be explained by the following scenario. In areas where precipitation occurs erroneously in the model and the assimilation of SRH adjusts the analyzed humidity so that the humidity is increased, then the erroneous precipitation in the model will increase even further, worsening the problem.

In the case of assimilation of SSM/I TPW and in the absence of other observations in the neighborhood, the vertical distribution of q is entirely controlled by the q background error covariances. The larger the background error is, the higher the weight of the SSM/I TPW will be. Figure 14 illustrates the difference fields of the zonally averaged ln(q) for the July 1996 experiments ln(q):C and ln(q):CS. These differences reflect the vertical distribution of background errors in ln(q) for which the largest errors are found in the tropical upper troposphere (Fig. 3). Around 10°N, the differences are largest above 850 hPa (maximum of −7.18%). In the SH, they are largest around 850 hPa (maximum of 13.10%). Since the distribution of humidity in the vertical is based on the background error covariances, these need to be known as accurately as possible. Because the radiosonde network is land-bound and by far dominates in the NH, it is believed that these may not be representative over the oceans.

c. *Impact on the Hadley circulation and mean meridional transport of humidity*

The mass flux stream function for the analyses was computed from the zonally averaged time-mean meridional velocity (Newell et al. 1972). As shown in Fillion et al. (1995), the adiabatic nonlinear normal mode initialization of the analyses was expected to decrease the intensity of the Hadley cell. For July 1996, the mass flux was computed for the control analyses and the corresponding initialized analyses. For this purpose, the fields at 0000 and 1200 UTC for each day of the month were averaged together. It was found that the maximum intensity of the Hadley cell was decreased by 6%.

Figure 15 illustrates the impact that assimilation of SRH had on the mass flux for the first 15 days of July 1996 (at 0000 and 1200 UTC). The assimilation of Humsat DPD retrievals increased the intensity of the Hadley circulation considerably more than when SSM/I TPW was assimilated. This is in agreement with the fact that much more precipitation is generated in the ITCZ due to the assimilation of Humsat DPD (Fig. 12c). The maximum intensity change was 23% for ln(q):CH (difference of maxima divided by the maximum value for ln(q):C and 14% for ln(q):CS. Recall that Humsat DPD is assimilated for only 40% of the area and therefore dramatically increases the Hadley circulation. The mean meridional transport of humidity (defined as the product of the zonal average of the time mean meridional velocity and the zonal average of the time-mean specific humidity) was also computed (not shown). The mean meridional transport of humidity for ln(q):CH was increased strongly just north of the equator (the maximum transport was increased by 8.6%) and also close to the surface in the subsidence zone 10°–25°S. For the ln(q):CS, the maximum increase in transport was 7% and located higher in the atmosphere (850–925 hPa).

d. *Comparison of NCEP reanalyses with the CMC analyses*

Since the NCEP reanalyses were readily available, the NCEP mass flux streamfunction and humidity fields were compared with those from the ln(q):C and ln(q):CS experiments. The NCEP reanalyses did not assimilate SSM/I TPW. Figure 16 shows the mass flux streamfunction for the month of July 1996 for NCEP reanalyses and experiments ln(q):C and ln(q):CS. The largest intensity of the Hadley cell for the ln(q):C is much closer to the surface than for the NCEP reanalyses and the NCEP Hadley cell center of maximum strength is shifted to the SH. Thus, these two systems appear quite different

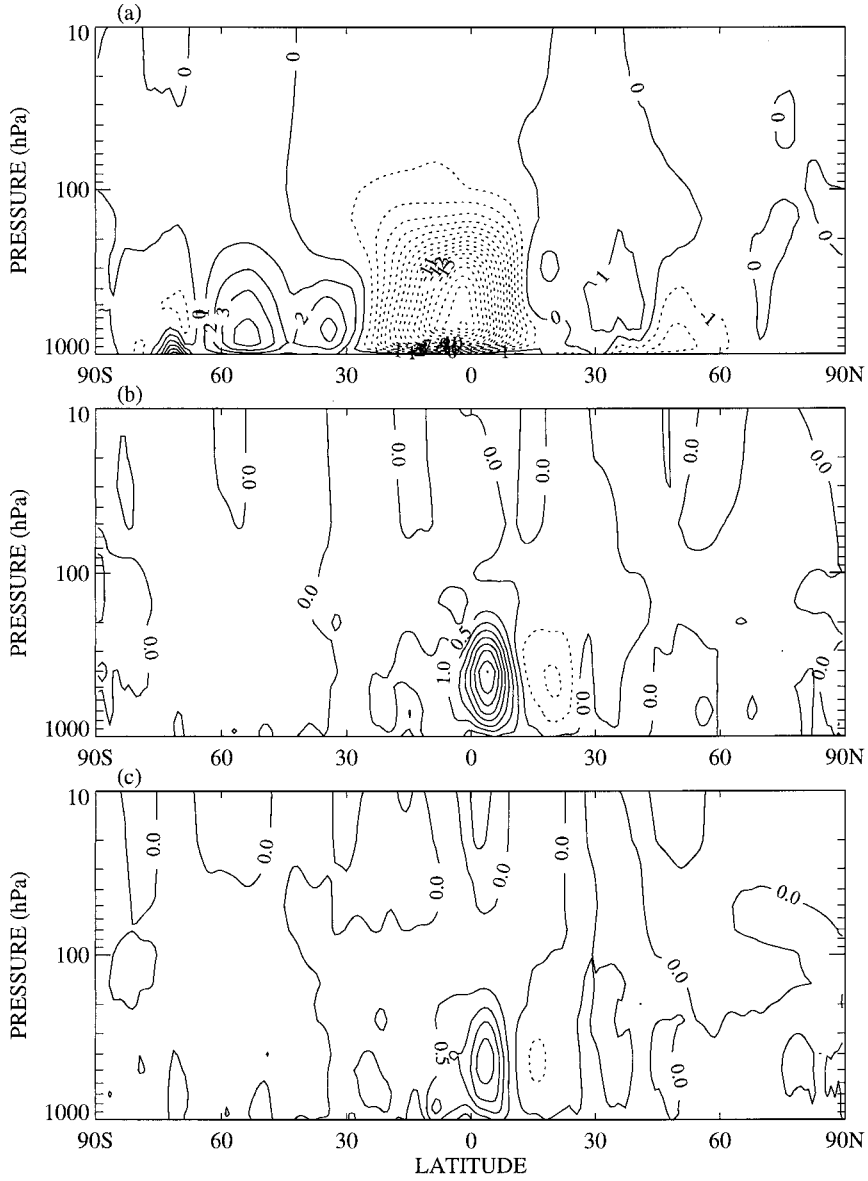

FIG. 15. Impact of assimilating SRH on the mass flux streamfunction for 1–15 Jul 1996 (0000 and 1200 UTC only). Units are 10^{10} kg s^{-1}: (a) ln(q):C, (b) ln(q):C − ln(q):CH, and (c) ln(q):C − ln(q):CS.

although maximum strengths are not too different. As discussed previously, adding SSM/I TPW increased the intensity of the Hadley cell and also the direct cell that is paired with the Hadley cell. The maximum intensity is also shifted higher (Fig. 16c). For the December case (not shown), the center of maximum strength coincides; however, the location of the maximum is again higher in the atmosphere for the NCEP reanalyses. Explaining the differences between NCEP reanalyses and CMC ln(q):C are beyond the scope of this paper.

Differences between NCEP reanalyses and ln(q):C zonally averaged q for July 1996 and December 1996 were computed (not shown). The NCEP reanalyses were much drier in the latitude band extending roughly from 30°S to 30°N except below ~900 hPa in the July SH case and in the winter NH where the atmosphere was more humid. Figure 17 illustrates TPW computed from the zonally averaged q for the NCEP reanalyses and the ln(q):C and ln(q):CS experiments. In the Tropics, the NCEP reanalyses are much drier than the ln(q):C and ln(q):CS experiments. As was discussed in section 4b(1), the agreement between the SSM/I TPW climatology and the ln(q):CS TPW was close (rmsd < 1.3 kg m^{-2}; Table 5), and, therefore, it is obvious that the

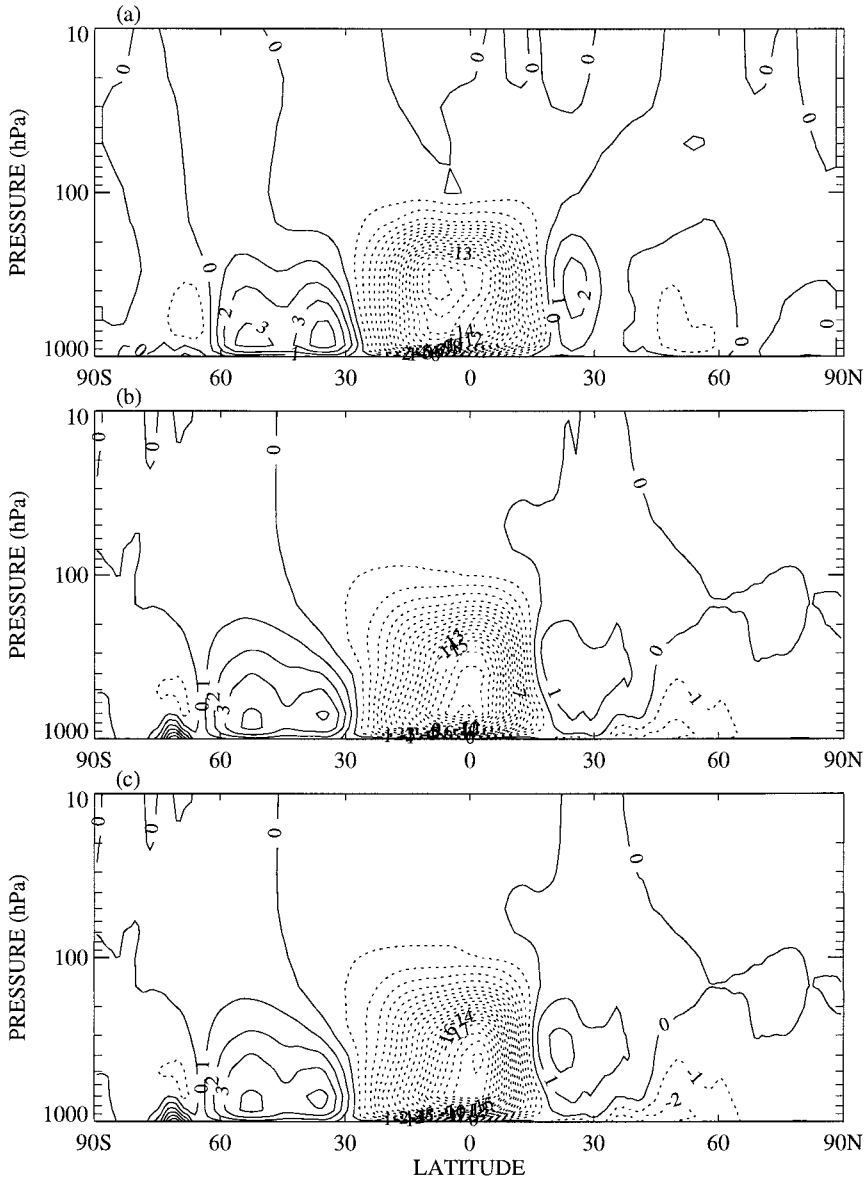

FIG. 16. Mass flux streamfunction for Jul 1996 (0000 and 1200 UTC only). Units are 10^{10} kg s^{-1}: (a) NCEP reanalyses, (b) ln(q):C, and (c) ln(q):CS.

NCEP reanalyses have a large dry bias in the Tropics compared with the SSM/I TPW climatology.

5. Conclusions

The objective of this study was to estimate the impact of assimilating SSM/I TPW retrievals on the CMC operational analyses and forecasts. Assimilation cycles were performed for the months of July 1996 and December 1996 with 5-day forecasts launched daily for the first two weeks of the months and 2-day forecasts for the remaining two weeks. Because of the lack of conventional measurements of humidity especially over the oceans, various verifying techniques were used to show that the assimilation of SSM/I TPW had a positive impact on the analyses and forecasts from the 3D-Var system.

For July 1996, collocations with a subset of island radiosondes over the oceans showed that both the analyses and forecasts of humidity were improved at and above 700 hPa in the Tropics. The winds also improved somewhat. In the SH extratropics the impact was not as large; the winds were not affected. A smaller positive impact was found for December 1996. However, TPW for the December control case also agreed better with the SSM/I TPW.

For July 1996, two more verifying techniques were used. The geopotential anomaly correlations showed an

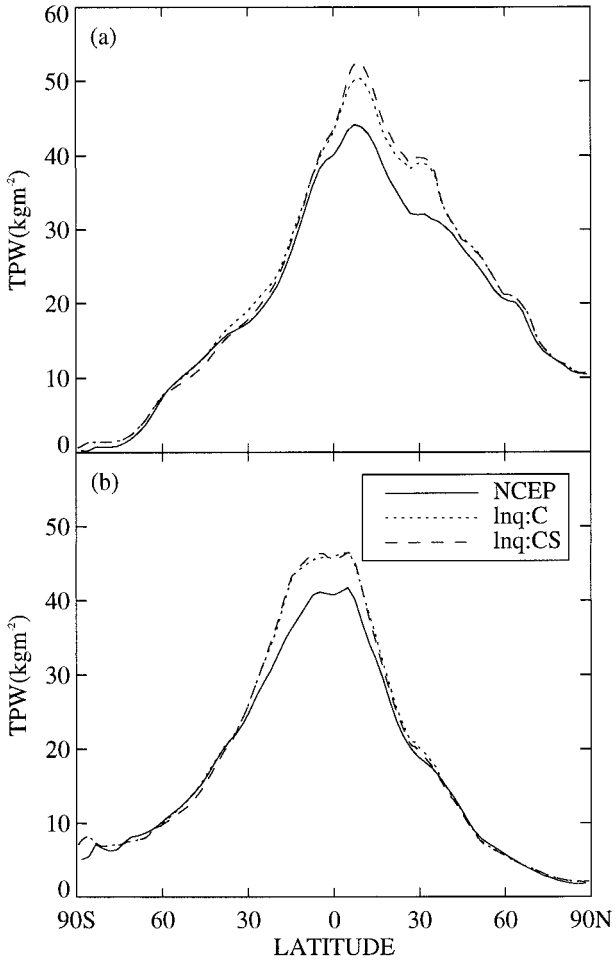

FIG. 17. TPW computed from zonally averaged specific humidity for pressure levels between 1000 and 300 hPa. NCEP in the legend stands for NCEP reanalyzed fields: (a) Jul 1996 (0000 and 1200 UTC only) and (b) Dec 1996 (0000 and 1200 UTC only).

increase of 1%–2% starting with the day 3 forecast in the Tropics and day 4 forecast in the SH extratropics. TOVS clear-sky TB simulations of the background fields showed a small reduction in SD.

The agreement between the SSM/I TPW climatology (monthly mean) and the analyzed q for the control case was quite good (rmsd of 2.98 kg m^{-2} in July 1996 and 2.64 kg m^{-2} in December 1996), which shows that the monthly average of the humidity analysis was already good. TPW of the control case was somewhat larger than for the SSM/I TPW climatology indicating a wet bias in the NWP model over the oceans between 60°S and 60°N. Taking into account the fact that the SEF model has a considerable precipitation spinup, comparison of the forecast precipitation rate with climatological observations (Huffman et al. 1997) indicated that this model has a hydrological cycle that is too active. The ITCZ–SPCZ precipitation band was too wide: the size of the large-scale subsidence zones was greatly underestimated.

The impact of assimilating SSM/I TPW in July 1996 was mainly to dry out the SH and increase TPW in the NH between 0° and 45°N. The NH increase in humidity was mainly due to an increase over a large area over the North Atlantic Ocean. The precipitation was also decreased in the SH and increased between 0° and 23°N. For December 1996, the impact was to decrease the precipitation both in the SH and NH midlatitudes and increase the humidity of the peak value of the ITCZ (increased between 10°S and 10°N). The net impact of assimilating SSM/I TPW was to slightly reduce the globally averaged precipitation rate. The precipitation in the large-scale subsidence zones was also closer to the observations.

The residence time of the impact of the humidity data was fairly short: less than 24 h in the midlatitudes and less than 48 h in the Tropics except for a small residual impact that lasts for the 5 days of the forecast. Thus, it did not take long before the model climatology took over. Assimilating SSM/I TPW accelerated the Hadley cell and increased the meridional transport of humidity in the Tropics.

It was also shown that the NCEP reanalyses for both the July 1996 and December 1996 months indicated that the atmosphere was considerably drier in the Tropics compared with the control cases and with the SSM/I TPW climatology.

Upgrades to the 3D-Var system would be highly desirable before assimilating SSM/I TPW operationally. Performing the analyses in model coordinates rather than in pressure coordinates would prevent one from having to use the first-guess surface pressure field to compute the integral of water vapor since the surface pressure would be analyzed. The analysis of humidity would also benefit from having a better temperature analysis at the surface. The specification of background error covariances and horizontal error correlations computed directly in $\ln(q)$ would also be desirable.

We are hoping that the Tropical Rainfall Measuring Mission (TRMM) endeavor will provide more accurate fields of precipitation in the Tropics. This should, among other things, allow for a better tuning and reduction of the precipitation spinup or spindown in NWP models. Since the control of the vertical distribution of the humidity increments for the SSM/I TPW happens only through the background error covariance specifications, it would also be helpful to assimilate radiances from humidity sounders such as TOVS, the Advanced TOVS, and the Special Sensor Microwave Water Vapor Sounder. Such impact studies will be performed in the future.

Acknowledgments. The author would like to thank A. P. McNally for suggesting the computation of TOVS TB and C. Chouinard for computing the TOVS TB and for other useful discussions. The author is also grateful to L. Phalippou, E. Gérard, and J. C. Derber for sharing some of their experience with the assimilation of SSM/I TPW.

REFERENCES

Alishouse, J. C., S. A. Snyder, J. Vongsathorn, and R. R. Ferraro, 1990: Determination of oceanic total precipitable water from the SSM/I. *IEEE Trans. Geosci. Remote Sens.,* **28,** 811–816.

Arpe, K., 1991: The hydrological cycle in the ECMWF short range forecasts. *Dyn. Atmos. Oceans,* **16,** 33–59.

Canadian Meteorological Centre, 1993: CMC reference guide. Dorval, PQ, Canada. [Available from Canadian Meteorological Centre, 2121 Trans-Canada Highway, Dorval, PQ H9P 1J3, Canada.]

Colton, M. C., and G. A. Poe, 1994: Shared processing program, Defense Meteorological Satellite Program, Special Sensor Microwave/Imager Algorithm Symposium, 8–10 June, 1993. *Bull. Amer. Meteor. Soc.,* **75,** 1663–1669.

Deblonde, G., and N. Wagneur, 1997: Evaluation of global numerical weather prediction analyses and forecasts using DMSP special sensor microwave imager retrievals. 1. Satellite retrieval algorithm intercomparison study. *J. Geophys. Res.,* **102** (D2), 1833–1850.

——, L. Garand, P. Gauthier, and C. Grassotti, 1995: Assimilation of SSM/I and GOES humidity retrievals with a one-dimensional variational analysis scheme. *J. Appl. Meteor.,* **34,** 1536–1550.

——, W. Yu, L. Garand, and A. P. Dastoor, 1997: Evaluation of global numerical weather prediction analyses and forecasts using DMSP special sensor microwave imager retrievals. 2. Analyses/forecasts intercomparison with SSM/I retrievals. *J. Geophys. Res.,* **102** (D2), 1851–1866.

Eyre, J. R., 1991: A fast radiative transfer model for satellite sounding systems. ECMWF Tech. Memo. 176, 28 pp. [Available from European Centre for Medium-Range Weather Forecasts, Shinfield Park, Reading, Berkshire RG2 9AX, United Kingdom.]

Fillion, L., H. L. Mitchell, and A. Staniforth, 1995: The impact of digital filter initialization technique in a global data assimilation system. *Tellus,* **47A,** 304–323.

Garand, L., 1993: A pattern recognition technique for retrieving humidity profiles from Meteosat of GOES imagery. *J. Appl. Meteor.,* **32,** 1592–1607.

——, and J. Hallé, 1997: Assimilation of clear- and cloudy-sky upper-tropospheric humidity estimates using *GOES-8* and *GOES-9* data. *J. Atmos. Oceanic Technol.,* **14,** 1036–1054.

Gauthier, P., L. Fillion, P. Koclas, and C. Charette, 1996: Implementation of a 3D variational analysis at the Canadian Meteorological Center. Preprints, *11th Conf. on Numerical Weather Prediction,* Norfolk, VA, Amer. Meteor. Soc., 232–234.

Huffman, G. J., and Coauthors, 1997: The Global Precipitation Climatology Project (GPCP) combined precipitation data set. *Bull. Amer. Meteor. Soc.,* **78,** 5–20.

Kalnay, E., and Coauthors, 1996: The NCEP/NCAR 40-Year Reanalysis Project. *Bull. Amer. Meteor. Soc.,* **77,** 437–461.

Ledvina, D. V., and J. Phaendtner, 1995: Inclusion of Special Sensor Microwave/Imager (SSM/I) total precipitable water estimates into the GEOS-1 data assimilation system. *Mon. Wea. Rev.,* **123,** 3003–3015.

Legates, D. R., 1994: Global and terrestrial precipitation: A comparative assessment of existing climatologies. *Int. J. Climatol.,* **15,** 237–258.

Liu, W. T., W. Tang, and F. J. Wentz, 1992: Precipitable water and surface humidity over the global oceans from special sensor microwave imager and European Center for Medium Range Weather Forecasts. *J. Geophys. Res.,* **97,** 2251–2264.

McNally, A. P., and M. Vesperini, 1996: Variational analysis of humidity information from TOVS radiances. *Quart. J. Roy. Meteor. Soc.,* **122,** 1521–1544.

Mitchell, H. L., C. Charette, S. J. Lambert, J. Halle, and C. Chouinard, 1993: The Canadian global data assimilation system: Description and evaluation. *Mon. Wea. Rev.,* **121,** 1467–1492.

Newell, R. E., J. W. Kidson, D. G. Vincent, and G. Boer, 1972: *The General Circulation of the Tropical Atmosphere.* Vol. 1. The MIT Press, 258 pp.

Petty, G. W., 1990: On the response of the SSM/I for atmospheric parameter retrievals. Ph.D. thesis, University of Washington, 252 pp. [Available from Department of Atmospheric Sciences, AK-40, University of Washington, Seattle, WA 98195.]

Phalippou, L., 1996: Variational retrieval of humidity profile, wind speed and cloud liquid-water path with SSM/I: Potential for numerical weather prediction. *Quart. J. Roy. Meteor. Soc.,* **122,** 327–355.

——, and E. Gérard, 1996: Use of precise microwave imagery in numerical weather prediction. Study report to the European Space Agency, 70 pp. [Available from European Centre for Medium-Range Weather Forecasts, Shinfield Park, Reading, Berkshire, RG2 9AX, United Kingdom.]

Ritchie, H., and C. Beaudouin, 1994: Approximation and sensitivity experiments with a baroclinic semi-Lagrangian spectral model. *Mon. Wea. Rev.,* **122,** 2391–2399.

Wentz, F. J., 1993: User's manual SSM/I antenna temperature tapes, Revision 2. RSS Tech. Rep. 120193, 70 pp. [Available from Remote Sensing Systems, 101 College Avenue, Suite 220, Santa Rosa, CA 95404.]

Wu, W.-S., and J. C. Derber, 1994: Inclusion of SSM/I precipitable water observations in the NMC spectral statistical-interpolation analysis system. Preprints, *10th Conf. on Numerical Weather Prediction,* Portland, OR, Amer. Meteor. Soc., 190–191.